Lidar Observations of Tropospheric Aerosols over northeastern South Africa during the ARREX and SAFARI-2000 Dry Season Experiments

James R. Campbell, * Ellsworth J. Welton, ** James D. Spinhirne, *** Qiang Ji, * Si-Chee Tsay, *** Stuart J. Piketh, + Marguerite Barenbrug, + and Brent Holben ***

* *Science Systems and Applications, Inc., Lanham, Maryland*
** *University of Maryland, Baltimore County*
*** *NASA Goddard Space Flight Center, Mesoscale and Atmospheric Processes Branch, Greenbelt, Maryland*
\+ *University of the Witwatersrand, Gauteng, South Africa*

Manuscript submitted to the *Journal of Geophysical Research*, May 2002.

Summary

A ground-based, eye safe Micropulse Lidar (MPL) instrument was deployed to the Skukuza Airport in northeastern South Africa in support of the Aerosol Recirculation and Rainfall Experiment (ARREX) – 1999 and South African Regional Science Initiative (SAFARI) – 2000 field campaigns. A diverse array of co-located passive remote sensing instrumentation, including a CIMEL sun-photometer, broadband solar flux radiometer and multi-filter shadowband radiometer, were also deployed. Measurements for both campaigns were collected during the dry season months of August and September when the region is subject to dense lower tropospheric haze due to the prevalence of biomass burning and sulfate emissions from power generator stations. Lidar observations provide vertical profiles of aerosol structure based on the principle of backscatter light as a function of time of detection after a given laser pulse. This paper summarizes the calculated optical parameters derived from both the lidar and passive datasets during SAFARI-2000. These include the lidar extinction to backscatter ratio, the spectral Angstrom Exponent, the 523 nm aerosol optical depth and the top of the surface aerosol layer height. A new algorithm is described for analyzing the lidar data built upon techniques described in earlier papers. From these parameters we characterize the temporal evolution through the experiment of the aerosol with regards to the influence of smoke particle loading in the surface aerosol layer. In particular, global observations of the surface aerosol layer extinction to backscatter ratio are very important to proposed data processing algorithms for satellite-based lidar projects. These algorithms will require a-priori knowledge of this parameter as a calibration reference point. A case study is also discussed summarizing observations made as a fresh smoke plume is observed advecting over the instrument array. Finally, observations of upper-tropospheric aerosols, possible dominated of elevated dust matter, during a two-week period from ARREX are described.

* *Corresponding author address:* James R. Campbell, c/o Code 912, NASA/Goddard Space Flight Center, E-mail: campbell@virl.gsfc.nasa.gov

Lidar Observations of Tropospheric Aerosols over northeastern South Africa during the ARREX and SAFARI-2000 Dry Season Experiments

James R. Campbell, [*] Ellsworth J. Welton, [**] James D. Spinhirne, [***] Qiang Ji, [*] Si-Chee Tsay, [***] Stuart J. Piketh, [+] Marguerite Barenbrug, [+] and Brent N. Holben, [***]

[*] *Science Systems and Applications, Inc., Lanham, Maryland*

[**] *Goddard Earth Sciences and Technology Center, University of Maryland, Baltimore County*

[***] *NASA Goddard Space Flight Center, Greenbelt, Maryland*

[+] *University of The Witwatersrand, Gauteng, South Africa*

[*] *Corresponding author address:* James R. Campbell, c/o Code 912, NASA/Goddard Space Flight Center, Greenbelt, MD, 20708. E-mail: campbell@virl.gsfc.nasa.gov

ABSTRACT

During the ARREX-1999 and SAFARI-2000 Dry Season experiments a micropulse lidar (523 nm) instrument was operated at the Skukuza Airport in northeastern South Africa. The lidar was co-located with a diverse array of passive radiometric equipment. For SAFARI-2000 the processed lidar data yields a daytime time-series of layer mean/derived aerosol optical properties, including extinction-to-backscatter ratios and vertical extinction cross-section profile. Combined with 523 nm aerosol optical depth and spectral Angstrom exponent calculations from available CIMEL sun-photometer data and normalized broadband flux measurements the temporal evolution of the near surface aerosol layer optical properties is analyzed for climatological trends. For the densest smoke/haze events the extinction-to-backscatter ratio is found to be between 60-80 sr^{-1}, and corresponding Angstrom exponent calculations near and above 1.75. The optical characteristics of an evolving smoke event from SAFARI-2000 are extensively detailed. The advecting smoke was embedded within two distinct stratified thermodynamic layers, causing the particulate mass to advect over the instrument array in an incoherent manner on the afternoon of its occurrence. Surface broadband flux forcing due to the smoke is calculated, as is the evolution in the vertical aerosol extinction profile as measured by the lidar. Finally, observations of persistent elevated aerosol during ARREX-1999 are presented and discussed The lack of corroborating observations the following year makes these observations both unique and noteworthy in the scope of regional aerosol transport over southern Africa.

1. Introduction

The climatic impact of biogenic, pyrogenic and anthropogenic surface emissions across the southern African sub-continent (described loosely here as that south of the 15° S latitude) has been the focus of much recent field research. The area is marked by significant industrial and domestic sulfate and carbon release. A dense network of generator stations situated along the Highveld of northeastern South Africa, responsible for most electrical power to the region, and the predominance of biomass burning, both as a domestic fuel source and in the form of savannah fires, are the most notable contributors [*Piketh et al.*, 1996]. Beginning with the 1992 South African Regional Science Initiative (SAFARI) field campaign, and continuing through numerous projects, including the 1999 Aerosol Recirculation and Rainfall Experiment (ARREX) [*Terblanche et al.*, 2000] and SAFARI-2000, many diverse datasets have been collected in the region through coordinated surface, airborne and satellite remote sensing and in-situ sampling. The goal of these efforts is the accurate characterization of regional aerosol evolution, transport and eventual deposition, and an improved understanding of the regional climatic and biological repercussions of its presence in the atmosphere [*Swap et al.*, 2002].

This article discusses observations made through co-located active and passive remote sensing at the Skukuza Airport in the Krueger National Park of northeastern South Africa during the ARREX and SAFARI-2000 Dry Season components. A Micropulse Lidar (MPL), described by *Spinhirne* (1993), is the primary instrument of focus. Low-powered, eye-safe, and autonomously operated, the ruggedized MPL instrument is quite amenable to remote field operating conditions [*Spinhirne et al.*, 1995]. The MPL is a single-

channel (523 nm), elastic backscatter lidar. Though low-powered, the MPL has been shown to detect nearly all forms of tropospheric cloud and aerosol. Sensitivities can reach as high as the lower stratosphere [*Spinhirne,* 1993]. MPL instruments have been used in numerous recent aerosol-related field experiments including the Indian Ocean Experiment (INDOEX) [*Welton et al.* 2002], the Aerosol Characterization Experiment-2 (ACE-2) [*Welton et al.*, 2000; *Powell et al.*, 2000], ACE-ASIA, and the Chesapeake Lighthouse and Aerosol Measurements for Satellites experiment (CLAMS) [*Smith et al.*, 2001]. They are able to run continuously for extended periods with only minor daily supervision [*Campbell et al.*, 2002]. In the current study, very little downtime was experienced during the two experiment periods.

A single-channel lidar is somewhat limited in stand-alone capability, particularly in light of more robust lidar systems with depolarization and multiple channel capacities used during SAFARI-2000 [*McGill et al.*, this issue], and previous African field campaigns [e.g., *Fuelberg et al.*, 1996, and *Browell et al.*, 1996]. The advantage of the MPL instrument is in its practicality (ease in remote deployment relative to typically bulkier systems), and ability to make full-time measurements. The vertical structure of aerosol and its evolution over extended timescales becomes more clearly evident. In addition to the lidar a diverse suite of passive instrumentation was operated simultaneously at the airport site [see *Tsay et al.*, this issue], and a CIMEL sun-photometer was situated less than a kilometer away in the Skukuza base camp. Integration of the datasets reveals much information on the optical characteristics of the incident aerosols, and well as qualitative information on the types of aerosols being observed.

In this presentation we examine the temporal evolution of regional dry-season aerosol optical parameters. Particular attention is given to the lidar-derived extinction-to-backscatter parameter (S-ratio). MPL instruments serve an ancillary purpose in collecting ground-validation datasets for the National Aeronautics and Space Administration (NASA) Earth Observing System (EOS) Geoscience Laser Altimeter System (GLAS) project [*Spinhirne et al.*, 2002]. Proposed GLAS data processing algorithms specify a-priori knowledge of this parameter [*Palm et al.*, 2001]. However, outside of modeling studies [e.g., *Ackerman et al.*, 1998], global characterization of regional S-ratio variation is lacking. The findings presented here, combined with similar measurements made by the Cloud Physics Lidar [*McGill et al.*, this issue] aboard the NASA ER-2 aircraft [*King et al.*, this issue] will prove very useful to this cause.

A case study is discussed detailing an evolving smoke plume from nearby biomass fires as observed advecting over the instrument array. This case is particularly unique as the smoke layers will be shown to have evolved within separate boundaries of two distinct stable thermodynamic layers. Variations in S-ratio measurements and spectral Angstrom exponent calculations allow us to separate distinct smoke and haze events observed during the SAFARI-2000 experiment with otherwise ordinary conditions. Combined with surface flux measurements, this case is fully characterized with mind kept to the potential for validation of modeling studies on downwind smoke plumes [e.g., *Trentmann et al.*, 2002] and regional smoke transport modeling overall..

Finally, we briefly discuss the unexpected observation of persistent elevated aerosol (throughout the troposphere) during ARREX. The persistence of significant elevated layers would prove bothersome to passive satellite algorithm retrievals that constrain

observed aerosol characteristics to the surface layer. Additionally, long-range aerosol transport modeling studies require regional characterization of the vertical aerosol structure to interpret model output. Note that cross-validation studies involving Skukuza MPL datasets and measurements from airborne instrumentation during SAFARI-2000 can be found in papers by *Schmid et al.* [this issue] and *McGill et al.* [this issue].

2. Instrument Setup and Data Processing

We briefly describe here the logistical setup for the MPL during both ARREX and SAFARI-2000, as they differed somewhat, resulting in various nuances to the post-calibration and processing of their respective datasets. Following the nomenclature of *Campbell et al.* [2002], the MPL instrument used during ARREX featured a V2.0 optical design, while that used in SAFARI-2000 was an updated V2.1 design. As this relates almost solely to 'afterpulse' cross-talk noise magnitudes (measured by the photon-counting detectors), the ARREX datasets are somewhat noisier (higher signal uncertainties) than those from SAFARI–2000. For reference, a picture of the instrument package common to both designs can be found in Fig. 1b of *Campbell et al.* [2002].

For the ARREX experiment, the MPL was housed in dual insulated containers, allowing for outdoor operation, though otherwise sheltered from environmental conditions. The package is pictured in operation in Fig. 1a. The two containers separated the fiber-coupled laser power supply, multi-channel scaler unit and system computer, from the optical transceiver. The containers were mated top (transceiver) and bottom using bracing pins, with two 50 cm diameter collared ducts allowed for wiring and air-flow circulation to be commonly shared. A broadband-coated, optically flat window was

mounted along the top face of the transceiver box. A 300 W capacity thermostatically driven thermo-electric cooler (seen on the side facing the camera in Fig. 1a) was responsible for maintaining a constant environment temperature inside the containers. The MPL had been measured in a laboratory setting to radiate approximately 250 W of heat during normal operations. However, when factoring in solar loading, and ambient temperatures (the containers were not perfectly air-tight, given the desire for somewhat regular manipulation of the system computer), the cooler failed to consistently maintain a steady state thermal surrounding during sunlight hours. As such, the instrument was placed between adjacent on-site aviation hangers to provide shading during most daytime hours. However, this did not solve the problem completely. *Welton et al.* [2002a] discuss difficulties in processing MPL data when the instrument is in a state of thermal flux, or under relative thermal stress. This point will be reconsidered below.

For SAFARI-2000, an MPL was placed inside the hanger on the left side of Fig. 1a, roughly 10 m behind the original ARREX set-up. Roughly speaking, this was an in-door arrangement. However, the hangers were not as well sealed as a typical insulated shelter. Still, the thermal difficulties experienced with the containers during the previous season were mostly overcome. A window mount was constructed on top of the hanger to allow for an optical-quality transmitting window to be attached. The instrument rested on the hanger floor with a ceiling-mounted fan placed in the upper hatch to inhibit window condensation. The instrument setup is shown in Fig. 1b.

Table 1 details the specifics of instrument operation for each experiment, including dates, uptime frequencies (based on 24 hr/day operation) and temporal/spatial resolution settings. Instrument correction terms were solved for using techniques outlined in

Campbell et al. [2002]. The Skukuza Airport rests upon relatively high ground. A clear horizontal sight line looking southwestward across the southern end of the runway made for a relatively easy calibration of the instrument overlap function in both experiments.

3. Data Processing

Normalization of the raw MPL data to a viable backscatter product requires accounting for ambient background light, instrument-specific correction terms, and solving for the system calibration coefficient as required by the lidar equation. *Campbell et al.* [2002] discuss the algorithm and assorted techniques used to develop the raw data to the point of uncalibrated backscatter (termed normalized relative backscatter, or NRB). *Welton and Campbell* [2002b] outline the methods for calculating uncertainties for this algorithm. Furthermore, *Welton et al.* [2002c] describe an algorithm for solving the absolute calibration coefficient (C), as well as indirectly derived optical parameters (i.e., backscatter and extinction cross-section profiles, optical depth profiles and layer-mean extinction-to-backscatter ratios), including uncertainties for all terms. These algorithms and techniques form the basis of the work presented here. Solving for C is accomplished using an independent measurement of the total column aerosol optical depth. During both experiments, an AERONET CIMEL sun-photometer was stationed less than 1 km from the Skukuza airport in the local base camp. Measurements from this instrument were used with an uncertainty taken to be +/- 0.01 [*Holben et al.* 1998]. *Campbell et al.* [2000] describe the variability of C over a diurnal cycle with the MPL. To insure accurate data processing with the lowest quantifiable uncertainties, we are restricted in

our analysis for this presentation to daytime periods where CIMEL measurements were available assuring a proper calculation of C.

The algorithm described in *Welton et al.* [2002b] employs a user-specified range above the surface aerosol layer from which to use for solving for C. After this calculation, the algorithm then searches for the top height of the aerosol layer in order to properly run a backward-Fernald numerical inversion [*Fernald*, 1984] to solve the two unknowns in the lidar equation (particulate backscatter coefficient, and particulate transmission). The result is a layer-mean value of S-ratio, and vertical profiles of extinction and backscatter. In order to automate this algorithm, we describe here a basic approach to first solving for the top of the aerosol layer, so as to choose a range for solving for C as near to the instrument as possible. This has a significant effect on decreasing the uncertainty in C that, in turn, improves the uncertainty in those subsequently derived parameters dependent upon it. In our analysis here, we utilize thirty-minute averages of NRB as centered around any reported CIMEL observation available for an experiment day through the AERONET database[1]. This greatly improves the signal-to-noise ratio for the MPL data and lowers overall uncertainty. A simple signal threshold filter developed for the MPL is applied to every profile, before inclusion within a period average, to avoid cloud contamination [*D. D. Turner*, 1998, personal communication].

To solve for the top of the aerosol layer we first find the range bin where the ratio of NRB signal to NRB signal uncertainty is less than 2.00. Roughly speaking, this relationship is essentially signal-to-noise ratio (SNR). However, the title SNR is typically

[1] The AERONET World Wide Web site is http://aeronet.gsfc.nasa.gov.

applied to the same ratio but for raw signal. Given that there are instrument correction terms and related uncertainties mixed into this new value it would be inappropriate to title it as such. But, the general correlation is still valid. This corresponding range is considered the top of the resolvable vertical column (i.e., the range to which there is reliable signal in the profile). As a value of 1.00 indicates the point of absolute uncertainty with regards to interpreting a single bin, a value of 2.00 is used to make the interpretation stringent.

For all range bins from the ground to the "noise bin" a value for C is solved for using the interpolated 523 nm AERONET optical depth (to solve the two-way particle transmission path), and a modeled molecular scattering profile. Next, the resolution of the profile is degraded to 150 m (two bins) and C is re-calculated for each bin (with lower uncertainty due to averaging) up to the "noise bin". Clearly this methodology is flawed, as C will not be correct applicable for every bin. But assuming that the entire aerosol layer is contained within a finite range in the area from the ground to the "noise bin", C will converge to a correct solution with range. In other words, C will be biased artificially high within the aerosol, but for the range past it, where backscatter is almost entirely molecular, the calculation will be accurate. Therefore, we use the minimum value found in the degraded resolution profile (less uncertainty than choosing a base value from the individual bin values) and use it as a base from which to normalize the individual bin values, such that

$$\chi(r) = C(r)/C^*(r^*) \qquad \textbf{(1)}$$

where C(r) is the C calculated at normal resolution, and C*(r*) is the base normalization value at the lower resolution (r*). The uncertainty of this relationship is given by

$$\partial\chi(r) = \chi(r)*\mathrm{SQRT}((\partial C(r)/C(r))\hat{}2 + (\partial C^*(r^*)/C^*(r^*))\hat{}2) \quad \mathbf{(2)}$$

In a noise-free environment, the first bin from the ground to the "noise bin" where $\chi(r)$ is equal to 1 could be considered free of aerosol and entirely composed of molecular components. However, in considering Eq. (2) we are restrained by the uncertainty of the signal and instead use the first bin where

$$\chi(r) < 1 + \partial\chi(r) \quad \mathbf{(3)}$$

to be the top of the aerosol layer. A 1.1 km range of bins beginning 300 m above the top of the aerosol layer (to offset small errors in the layer top search) is then designated as the calibration zone for solving C [*Welton et al.*, 2002b].

This somewhat simple technique does not differentiate between individual aerosol layers, rather it finds the top of the highest aerosol layer as determined by the first range bin containing signal derived from only molecular-scattering, as constrained by uncertainty. Two scenarios can occur which undermine the methodology. First, if separate elevated layers are present above the surface layer, such that a well-defined "clear slot" is evident in the signal profile, the algorithm will not search for their presence. Instead, it will solve for C assuming that the CIMEL AOD measurement was due entirely to transmission in the surface layer. Second, if the "noise bin" were to be

found before reaching the top of the surface layer (e.g. dense hazes), the algorithm would default to that point as representing the top of the layer. If this range were not within 300 m of being accurate, the algorithm would incorrectly choose the calibration zone. Both of the above circumstances produce clearly erroneous values of C that are easily filtered out. For the SAFARI-2000 datasets (discussed in Section 4.1), less than 10% of the data was removed as a result. Efforts are underway to more clearly delineate particulate layers within the vertical MPL signal profile, however this method easily facilitates the automated processing of the robust MPL datasets.

4. Results and Discussion

As noted, MPL instruments have been found to be very sensitive to their ambient thermal operating environment. Under immoderate temperatures, instrument correction terms lose their validity, as the integrity of the instrument optical path is compromised due to thermal expansion/contraction in the system. During ARREX, the instrument was subjected to wildly fluctuating temperatures making automated processing of the datasets impractical. Operating conditions during SAFARI-2000 were much more accommodating, and these data are relied upon for the quantitative discussion and interpretation found in Sections 4.1 and 4.2.

4.1. Optical Parameters Derived During SAFARI-2000

During SAFARI-2000, the MPL was operated from 18 August through 22 September. Low clouds spoiled much of the last week of this period, so we focus here on the period through 13 September inclusive. Figure 2 shows processed automated algorithm output;

the surface aerosol mean S-ratio value (with error bars), and top of the aerosol layer height. Two additional parameters are shown as derived from available CIMEL spectral optical depth information, the 523 nm aerosol optical depth (AOD) and the Angstrom exponent (AE). 523 nm AOD values were solved for using a second-order polynomial fit versus wavelength where at least four of the seven available CIMEL channels (between 340 and 1020 nm) reported data. Values of AE were similarly derived though using a traditional power law curve-fit. In consideration of instrument thermal/optical stability, only those observations where the MPL instrument temperature was less than 27.8 deg Celsius are presented (chosen based on prior experience with this particular instrument).

Previous researchers have shown that the composition of the aerosol common to the region is highly complex, with many factors influencing it at any given time and place [e.g. *Piketh et al.* 1996]. Over a span of 25 days, it is nearly impossible to interpret the lidar data alone and accurately characterize the types of aerosols are being sampled (which is extremely important if one wishes to draw any climatological conclusions). With respect to advecting smoke from biomass burning events, this is particularly relevant. Integration of the CIMEL observations simplifies this, or at least allows us some hope to grouping days/cases/periods with regards to a more robust analysis of the mean optical parameters available.

Stable synoptic conditions dominated the latter part of August, into early September allowing for many data points. The period 18 - 29 August (fractional days 231 – 242) is marked by a progressive pattern. The aerosol layer top height peaks near 5.0 km on 21 August (day 234), with corresponding peaks in AOD and AE, and slowly subsides to 4.0 km near the 29th. AE values approach 2.0, and are among the highest observed during the

experiment. These measurements are consistent with a gradual increase in local smoke concentrations, contributing to an overall increase in aerosol loading, followed by a return to a more homogenized mix, which appears indicative of otherwise normal background conditions. The trending of the S-ratio is similar, with values from 40 to 60 sr^{-1}, maxing out on average near 80 sr^{-1}. Note that as the AOD increases, the relative uncertainty in the S-ratio similarly increases. As the lidar transmission through the surface aerosol layer decreases with higher AOD, less signal from above the layer leads to higher uncertainty in C, and therefore a higher uncertainty in the subsequent optical calculations.

The three days of 1 - 3 September (days 245 – 247) are heavily influenced by smoke (to be examined further below). The surface aerosol layer swells to near 5.0 km, AE values peak again near 2.0, the AOD reaches a maximum at 0.60 and the S-ratio is generally between 60 to 80 sr^{-1}, though uncertainties are quite high in these latter cases. This period ended abruptly as a synoptic disturbance moved through the area inducing low and mid-level cloudiness. The system was strong enough to scour out the heavy smoke and haze from the surface layer. By 9 September (day 253) the AOD had dropped to 0.20, and the aerosol layer top height was near 3.0 km. More notably, AE values plunged to near 1.0, and the S-ratio was calculated at roughly 40 sr^{-1}. It can be concluded that a complete recycling of the aerosol occurred. A more maritime-based aerosol composition may have influenced conditions, given the near proximity of the ocean and the preference of some common low-level circulations along the Lowveld region [*Piketh et al.*, 1996; *Tyson et al.*, 1996; *Garstang et al.*, 1996]. A return to the more homogenized mix follows though the end of the experiment.

To put these measurements in some perspective, Fig. 3 shows a plot of averages of the 523 AOD and spectral AE (with standard deviations) for the period 15 August through 15 September inclusive during the years 1998 to 2001. With respect to AE, and to a lesser degree AOD, the 2000 season was somewhat unusual. The increase in both parameters over the previous two years is consistent with a decrease in the particle size distribution of the aerosol, and an increase in overall loading. And, these findings support an increased influence of biomass burning aerosols [*Reid et al.*, 1998; *Remer et al.*, 1996].

In Fig. 4a is a comparison of S-ratio calculations to their corresponding AE value for the data points shown in Fig. 2. A comparison of AOD versus AE values corresponding to the cases in Fig. 4a is shown in Fig. 4b. The AE parameter is somewhat less ambiguous than the S-ratio, and is therefore somewhat more reliable parameter for interpreting observed aerosol type over time. AE is directly related to the slope of a Junge-type size distribution. The S-ratio is dependent upon the aerosol phase function and the single scatter albedo, and therefore is sensitive not only to changes in particle size, but also shape and refractive index. And, as aerosol species also have varying hydroscopic properties, particle size, shape, and refractive index are all dependent upon relative humidity to some degree. Considered as such, the relatively wide spread in Fig. 4a is to be expected given the chaotic nature of the regional aerosol composition and structure. For instance, the irregular advection of biomass burning aerosols contrasted with otherwise normal conditions should realistically be expected to cause variability in S-ratio measurements on timescales potentially as often as every few minutes.

It is conceded that some outlying points from the otherwise reasonable regression mean in Fig. 4a are likely due to the automated algorithm failing to properly assign the

top of the aerosol layer height, and therefore improperly applying the inversion methodologies. Cloud contamination, either in the normalized lidar profile, or as a bias in the reported CIMEL AOD spectral profile, could also be a factor. However, separate papers by *McGill et al.* [this issue] and *Schmid et al.* [this issue] show the MPL algorithm output (including profiles of extinction coefficient as well as S-ratio calculations) to be in good overall agreement with other instruments running concurrently near or at Skukuza at various points during the experiment. These results also agree reasonably with previous measurements [e.g., *Welton et al.*, 2000; *Voss et al.*, 2001]. Note, a chaotic spread similar to Fig. 4a was coincidentally (or perhaps not) observed in ER-2 lidar measurements made during the Smoke Clouds and Aerosols – Brazil (SCAR-B) experiment [*W. D. Hart*, 2002, personal communications].

Full closure in understanding the sources and effects of aerosol in the southern African region would include linking sources and transport of aerosol to types and distributions, and then to their optical properties. Given the broad based observations made over the last ten years this has become very possible, though well beyond the scope of the subject work. However, a more limited approach could be taken by interrelating the optical measurements themselves. For aerosol, the absorption as quantified by the wavelength dependent single scatter albedo is the major determining factor for a given AOD of the aerosol induced heating rate and surface shortwave flux forcing. Both the S-ratio and the ratio of broadband shortwave diffuse to direct flux depend on the aerosol absorption. For the S-ratio, it is well known that increasing the imaginary index, and thus absorption, suppresses the backscatter cross section. The suppression shows up most dramatically in Mie calculations for spherical particles. For a given size distribution and

real index, the S-ratio can change by an order of magnitude. In past studies (e.g., Spinhirne 1980) attempts have been made to estimate the imaginary index of aerosol from S-ratio measurements. Although there are large uncertainties introduced by particle non-sphericity, composition and unknown size distribution, results do fit a realistic model. Sky brightness is expected to decrease as aerosol absorption increases. A "dark" aerosol of lower single scattering albedo should lower the diffuse SW flux. Although there is also a scattering phase function effect, the primary impact of increasing the imaginary index in calculation is to lower the diffuse to direct ratio due to absorption. Surface albedo is also a major influence on the diffuse to direct raio and must be known for a quantitative assessment. A higher surface albedo would magnify the aerosol absorption influence.

In Fig. 5 is shown a comparison of the measured diffuse to direct shortwave flux ratio versus the corresponding path normalized CIMEL AOD (multiplied by airmass) for three distinct grouping of derived S-ratio (less than 55, between 55 and 75 and greater than 75 sr^{-1}. The expected dependence of lower S-ratio with a higher diffuse to direct SW radiance raio is clearly evident. Running model calculations based on an aerosol size distribution and a range of particle optical parameters can allow a quantitative analysis of these parameters. If the analysis agrees, as is seen at least qualitatively in Fig. 5, there would be fair confidence that the optical properties of the observed aerosol cases were understood. This would involve simultaneous observations from available aircraft particle measurements supplemented, where needed, by derived size distributions from available CIMEL data. Such work will be investigated further.

4.2 Advecting Smoke Layer Case Study: 1 September 2000

In this section we analyze observations made on 1 September 2000 (fractional day 245), when smoke from upwind biomass burning was observed advecting over the airport site. Figure 6 is a three-channel (.66 μm, .55 μm, and .47 μm) composite image of Level 1B Moderate Resolution Infrared Spectrometer (MODIS) data taken aboard the NASA EOS Terra satellite between 0900 – 0905 UTC from this day (approximately 245.37). The Skukuza Airport (24.97° S, 31.58° E) is denoted in the image by a white dot. The satellite pass was centered well to the west of Skukuza (note the edge of the data swath on the right side of the image), so the resolution in the area of interest has been compromised to some degree. However, many fires and their resulting plumes are evident. The highest concentration of fires is confined to a 3° by 3° grid directly north of Skukuza.

In Fig. 7, NRB data are displayed for the entire day. The surface aerosol layer is confined to the first 4.00 km AGL. Balloonsonde measurements from 0500 and 1200 UTC are shown in Fig. 8a-b. The top of the layer is capped by a slight temperature inversion detected near 580 mb in the early morning (Fig. 7a, fractional day 245.2076) and near 560 mb during the mid-afternoon (Fig. 8b, 245.4993). Measurements from the passive instrument array at the airport are concatenated into Fig. 9a. These include total, direct and diffuse broadband flux measurements, 866 nm multi-filter shadowband radiometer AOD values (more data points than the CIMEL for this comparison), and "airmass" calculations (defined as the inverse cosine of the solar zenith angle). Figure 9b compares total broadband flux versus airmass. Both figures are for the daylight hours only. Figure 10 is an expansion of Fig. 2 for the subject day, with MPL algorithm output

supplemented by corresponding CIMEL measurements. Finally, in Fig. 11 are three profiles of the extinction cross-section as derived from the MPL measurements for the early morning (245.23), mid-afternoon (245.50), and late afternoon (245.60).

What is unique in this event is that the advancing smoke plume, as witnessed at Skukuza, developed within two thermally separated layers. Aside from the upper inversion cap, a strong near-ground inversion is present in both radiosonde profiles (Fig. 8). During the morning it was situated near 1.00 km. By afternoon, thermal expansion of the layer caused it to lift to near 1.50 km. A clear delineation of the layers throughout the day is evident in both the NRB data image (Fig. 7), and the derived extinction profiles (Fig. 11).

From the NRB data, in the early hours of the day aerosol in the upper layer was well mixed, though wisp-like strands of smoke could be seen near 245.10. In the lower layer, a denser aerosol was detected. Though the first available sounding profile (Fig. 8a) came a few hours later, it is likely that the extremely stable thermal structure measured in the lower layer at that time prevailed earlier as well. With the sunrise (near 245.20) an evolution of the layer to the more convectively unstable one seen in the afternoon (Fig. 8b) commenced. This can be seen in the NRB data as the aerosol collects near the inversion cap height (convective mixing) with time. Gradually the layer dissipates by 245.40. A snapshot of this evolving structure is seen in the first extinction profile (Fig. 11a) where a peak calculation over 0.30 km^{-1} is found in the lower layer, while the upper layer displayed varying intensities under 0.10 km^{-1}. AE values beginning after sunrise (Fig. 10) are near 1.50, suggesting that the effective layer composition was likely a relatively common one (relative to Fig. 3 and Fig. 4a).

Through the middle of the day (245.50), AE values increased, as did the 523 nm AOD. The MODIS image, though three hours earlier, showed that the corridor within the Lowveld was completely covered with varying degrees of smoke. However, denser concentrations were not yet in the immediate vicinity of Skukuza. The NRB data continues to indicate that the smoke was almost exclusively confined to the upper layer. A peak extinction coefficient from the midday profile near 0.20 km^{-1} was detected at 2.50 km (Fig. 11b). The temporal evolution of the lower layer structure from sunrise on does not indicate any onset of significant smoke. This is presumably due to higher wind speeds above the near-ground inversion causing increased particle advection in the upper layer (wind data was not available from the balloonsonde data). S-ratio values, highly variable earlier in the day (no doubt influenced by the intermittent smoke wisps), converge at this time to a value near 60 sr^{-1}.

Two hours later (245.650), smoke embedded in the lower layer reached the airport. AE values peaked near 1.7, while the 523 nm AOD approached 0.8. The corresponding extinction profile (Fig. 11c) shows the remarkable change in the structure of this layer. This late afternoon event marked one of the densest smoke events in terms of AOD observed during the experiment. Stabilization of the S-ratio values indicates a temporarily homogeneous aerosol composition. As such, it makes sense that the location of the upwind burning was in somewhat close proximity as the MODIS imagery validates. Turbulent mixing over the lifetime of the plume had yet to have much effect in entraining dissimilar air, thereby inducing fluctuation in this measurement.

The change in broadband forcing at the ground caused by the smoke was approximately -50 W/m^2, when compared to corresponding airmass values from earlier in

the day (i.e., when the sun was rising versus when the sun was setting) (Fig. 9b). As smoke was present in the upper layer during this earlier time, we estimate that the overall forcing of the smoke relative to the otherwise common background aerosol was actually somewhat higher than this amount.

Tyson et al. [1995, 1996] discuss climatological air transport patterns over southern Africa in the lower troposphere, and corresponding aerosol recirculation in conjunction with the convective boundary layer. They also identify climatological trends in observed thermal inversion boundaries. Of note, *Tyson et al.* [1996] use downward-looking lidar observations made in SAFARI-92 to correlate aerosol concentrations with significant vertical thermodynamic structures. They found comparable discontinuities in aerosol concentration with each incident layer. Though they did not document a case such as this.

Transport-modeling efforts involving smoke in such a unique thermal environment face a daunting task. The available data limits us from deriving any potential optical differences between the two layers. But we can safely assume that as the case unfolds with time, a continued delineation of the layers will lead to two uniquely modified aerosol types. What is clear is that a significant amount of smoke has reached the upper thermal layer, and that it is advecting quickly upstream from that trapped in the lower layer. Models will need accurate characterization of the efficiency at which the plume punches through the first inversion (i.e., buoyancy), not to mention proper initialization of the ambient thermal environment itself. Finally, the evolution of the aerosol composition would need to be accurately depicted in response to entrainment and modification.

4.3 Elevated Aerosols during ARREX

While the MPL data from ARREX were not suitable for automated algorithm processing, we wish to highlight a finding from these data that contrasted with those collected during the 2000 campaign. Specifically, the presence of persistent elevated aerosols. In Fig. 11 are MPL NRB data from 7 September 1999. While cloud and heavy aerosol loading was observed during the first two-thirds of this day, by early evening the upper-troposphere could be identified and much aerosol structure was evident. This day represents one example amidst a near two-week period (between 24 August and 7 September) where detectable aerosol was measured well above the common surface stable layers. No such cases of upper-tropospheric aerosol could be found in the SAFARI-2000 datasets.

Unfortunately, it is not readily obvious what the aerosol is composed of. Interpretation of the available lidar and passive data is otherwise ambiguous. In-situ aircraft measurements were made, but the data were not conclusive. Ozone concentrations were found to be above normal background levels, which are indicative of biomass burn remnants. The possibility of downstream advection from fires in southern Zambia and neighboring countries exists, though the lack of corroborating observations the following year raises uncertainty in this scenario. One other possibility is the existence of elevated dust matter; perhaps from the arid environments of the west coast of Africa or even beyond, transported by rapid upper-tropospheric jet stream flow far down stream from its source. AE calculations from available CIMEL data were quite low during this period with respect to the measurements detailed above from 2000. Common values were near 1.0, which are inconsistent with observations associated with biomass burning events

observed in 2000 and more characteristic (at least in relative magnitude to normal background conditions) of dust. Though no sounding data was available for early September, the apparent structure in Fig. 11 suggests that the particles were stratified along thermal boundaries. This would seem consistent with a prolonged presence, whereby newly introduced particulate would likely show some turbulent (mixing) structure. Attempts to run optical algorithm retrievals on these data aside from the automated routines were limited. When successful, the contributions of these aerosols to column optical depths amounted to no more than approximately 0.05 ± 0.03 at 523 nm (not shown). The high uncertainties are the result of the very high uncertainties derived with the corresponding layer mean S-ratio value.

Though we cannot offer a definite classification of nature of these elevated aerosols, their striking contrast in vertical structure and temporal extent to the more robust observations made the following year are at worst still noteworthy. The statically stable nature of the southern African lower-troposphere would appear to inhibit the prolonged protrusion of surface-elevated particulates well above the height of the upper-most common inversion layer (~ 500 MB). Considering the scenario of biomass burning, it would seemingly (relative to 2000) require an impressive event to generate the significant buoyancies capable of penetrating the inversions over an extended period. However, it is well understood that wind-driven dust events commonly induce particulate transport on global scales. At any rate, those regional transport-modeling efforts buoyed by the observations made in the SAFARI-2000 experiment should give careful consideration to these findings.

5. Conclusions

In this paper we summarize and compare observations taken during August and September for 1999 and 2000 at the Skukuza Airport in northeastern South Africa using a Micropulse Lidar instrument co-located with passive radiometric equipment. The measurements were made in concurrence with the ARREX and SAFARI-2000 field campaigns. The purpose of these measurements enhance understanding of optical properties, both layer mean and vertically structured, of regional aerosols, which are heavily influenced by sulfate emissions and biomass burning. Specifically, regional characterization of the lidar-derived layer-mean extinction-to-backscatter ratio is of particular importance to satellite-based lidar programs as calibration reference points. We have shown that during the dry-season months, there is some variability in this parameter based on synoptic conditions and aerosol loading and the proximity of biomass burning. Additionally, we detail a case study during SAFARI-2000 where the onset of smoke from a nearby fire is observed advecting over the instrument array within two distinct thermal layers. We show the evolution of this event both in vertical profiles of particulate extinction cross-section, layer-mean S-ratio, and with respect to surface broadband flux and sun-photometer measurements. Finally, we show measurements of persistent elevated aerosols observed during ARREX. The composition of these aerosols is not immediately clear. Interpretation of available data indicates a likelihood that the aerosol was mostly elevated dust particles advected far downwind from a source region.

Deployment of the MPL instruments for these experiments was coordinated through the recently formed NASA EOS Micropulse Lidar Network project (MPL-Net) [*Welton et al.*, 2001]. The MPL-Net program was designed to establish a global network of MPL

systems of long-term climatological cloud and aerosol research. In the coming years, instruments will be deployed at pre-existing AERONET field sites to supplement co-located sun-photometer measurements with profiles of vertical structure. Additionally, field campaigns will be supported as deemed relevant. Datasets described in this paper are available on-line, and potential users are encouraged to visit the project website to make specific inquiries[2].

Acknowledgments

MPL research at the Goddard Space Flight Center is funded by the National Aeronautics and Space Administration (NASA) Earth Observing System, and the NASA Sensor Intercomparison and Merger fund for Biological and Interdisciplinary Oceanic Studies. The authors wish to thank Dennis L. Hlavka, William D. Hart, Dr. Matthew McGill, Timothy D. Berkoff, and V. Stan Scott for helpful insights and dedicated work on the MPL program, and Kristy Ross and Christoph Bollig for their assistance with the instruments in the field. We also thank Mark Gray (NASA GSFC) of the MODIS Atmosphere Team, who provided the composite image from 1 September 2000.

References

[2] The MPL-Net World Wide Web site can be accessed at http://virl.gsfc.nasa.gov/mpl-net/

Ackermann, J., 1998: The extinction-to-backscatter ratio of tropospheric aerosol: A numerical study, *J Atmos. Oceanic Technol.*, **15**, 1043-1050.

Browell, E.V., and Coauthors, 1996: Ozone and aerosol distributions and air mass characteristics over the South Atlantic Basin during the burning season. *J. Geophys. Res.*, **101**, 24043-24068.

Campbell, J. R., D. L. Hlavka, E. J. Welton, C. J. Flynn, D. D. Turner, J. D. Spinhirne, V. S. Scott, I. H. Hwang, 2002: Full-time, eye-safe cloud and aerosol lidar observation at Atmospheric Radiation Measurement Program Sites: Instruments and data processing. *J. Atmos. Oceanic Technol.*, **19**, 431-442.

Campbell, J. R., D. L. Hlavka, J. D. Spinhirne, R. Ferrare, and D. D. Turner, 2000: Automated aerosol retrieval algorithms for ARM Micro Pulse Lidars. In *Preprints of Symposium on Lidar Atmospheric Monitoring*, American Meteorological Society, 71-74.

Fernald, F.G., 1984: Analysis of atmospheric lidar observations: Some comments. *Appl. Optics*, **23**, 652-653.

Fuelberg, H. E., J. D. VanAusdall, E. V. Browell, and S. P. Longmore, 1996: Meteorological conditions associated with vertical distributions of aerosols off the west coast of Africa. *J. Geophys. Res.*, **101**, 24,105-24,115.

Garstang, M., P. D. Tyson, R. Swap, M. Edwards, P. Kallberg, and J. A. Lindesay, 1996: Horizontal and vertical transport of air over southern Africa. *J. Geophys. Res.*, **101**, 23,721-23,736.

Holben, B. N., and Coauthors, 1998: AERONET – A federated instrument network and data archive for aerosol characterization. *Remote Sens. Environ.*, **66**, 1-16.

King, M. D., S. Platnick, and C. O. Moeller, 2002: Remote sensing of smoke, land and clouds from the NASA ER-2 during SAFARI 2000. *Journal of Geophysical Research*, submitted.

Kotchenruther, R. A. and P. V. Hobbs, 1998: Humidification factors of aerosols from biomass burning in Brazil. *J. Geophys. Res.*, **103**, 32,081 – 32,089.

Le Canut, P., M. O. Andreae, G. W. Harris, F. G. Wienhold, and T. Zenker, 1996: Aerosol optical properties over southern Africa during SAFARI-92. *Biomass Burning and Global Change*, J. Levine, Ed., MIT Press, 441-459.

McGill, M. J., D. L. Hlavka, W. D. Hart, E. J. Welton, and J. R. Campbell, 2002: Airborne lidar measurements of optical properties of aerosol optical properties during SAFARI-2000. *J. Geophys. Res.*, submitted.

Palm, S. P., W. D. Hart, D. L. Hlavka, E. J. Welton, and J. D. Spinhirne, 2001: GLAS Atmospheric Data Products: Algorithm Theoretical Basis Document V4.1. NASA Goddard Space Flight Center, Greenbelt, MD, 111 pps.

Piketh, S. J., H. J. Annegarn, and P. D. Tyson, 1999: Lower tropospheric aerosol loadings over South Africa: The Relative contribution of Aeolian dust, industrial emissions, and biomass burning. *J. Geophys. Res.*, **104,** 1597-1607.

Powell, D. M., J. A. Reagan, M. A. Rubio, W. H. Erxleben, and J. D. Spinhirne, 2000: ACE-2 multiple angle micro-pulse lidar observations from Las Galletas, Tenerife, Canary Islands. *Tellus B*, **52,** 651-660.

Reid, J. S., P. V. Hobbs, R. J. Ferek, D. R. Blake, J. V. Martins, M. R. Dunlap, and C. Liousse, 1998: Physical, chemical, and optical properties of regional hazes dominated by smoke in Brazil. *J. Geophys. Res.*, **103,** 32,059 – 32,080.

Remer, L. A., Y. J. Kaufman, and B. N. Holben, 1996: The size distribution of ambient aerosol particles: Smoke versus Urban/Industrial aerosol. *Biomass Burning and Global Change*, J. Levine, Ed., MIT Press, 519 – 530.

Schmid, B., and Coauthors, 2002: Coordinated airborne, space borne, and ground based measurements of massive, thick aerosol layers during the SAFARI-2000 Dry Season Campaign. *J. Geophys. Res.*, submitted.

Smith, W. L., and Coauthors, 2001: The Chesapeake Lighthouse and Aircraft Measurements for Satellites (CLAMS) Experiment. *11th Satellite Meteorology and Oceanography Conference*, Madison, WI, October 2001.

Spinhirne, J. D., Reagan, J. A., and Herman, B. A., 1980: Vertical distribution of aerosol extinction cross-section and inference of aerosol imaginary index in the troposphere by lidar technique. *J. Appl. Meteor.*, **19,** 426-438.

Spinhirne, J. D., 1993: Micro pulse lidar. *IEEE Trans. Geo. Rem. Sens.*, **31,** 48-55.

Spinhirne, J. D., J. A. R. Rall, and V. S. Scott, 1995: Compact eye safe lidar systems. *Rev. Laser Eng.*, **23**, 112-118.

Spinhirne, J. D., and Coauthors: Atmospheric measurements by the Geoscience Laser Altimeter System (GLAS) Earth Observing System mission. *Bull. Amer. Meteorol. Soc.*, submitted.

Swap, R. J., and Coauthors, 2002: The Southern African Regional Science Initiative (SAFARI 2000) dry-season field campaign: an overview. *South African Journal of Science*, submitted.

Terblanche, D. E., M. P Mittermaier, S. J. Piketh, R. T. Bruintjes, and R. P. Burger, 2000: The Aerosol Recirculation and Rainfall Experiment (ARREX): An initial study on aerosol-cloud interactions over South Africa. *S. Afr. J. Sci.*, **96,** 15-21.

Trentmann, J., M. O. Andreae, H. –F. Graf, P. V. Hobbs, R. D. Ottmar, and R. Trautmann, 2002: Simulation of a biomass-burning plume: Comparison of model results with observations. *J. Geophys. Res.*, **107,** 410-414.

Tsay, S. –C., and Coauthors, 2002: Surface remote sensing during SAFARI-2000 dry season and effects of aerosol humidification on visual air quality. *J. Geophys. Res.*, submitted.

Tyson, P. D., M. Garstang, and R. Swap, 1995: Large-scale recirculation of air over southern Africa. *J. Appl. Meteorol.*, **35,** 2218-2236

Tyson, P. D., M. Garstang, R. Swap, P. Kallberg, and M. Edwards, 1996: An air transport climatology for subtropical southern Africa. *Intl. J. of Climatology*, **16,** 265-291.

Voss, K.J., E.J. Welton, P.K. Quinn, J. Johnson, A. Thompson, and H. Gordon, 2001: Lidar measurements during Aerosols99. *J. Geophys. Res.*, **106,** 20821-20832.

Welton, E. J., and Coauthors, 2000: Ground-based lidar measurements of aerosols during ACE-2: Instrument description, results and comparisons with other ground-based and airborne measurements. *Tellus B*, **52,** 635-650.

Welton, E. J., K. J. Voss, P. K. Quinn, P. J. Flatau, K. Markowicz, J. R. Campbell, J. D. Spinhirne, H. R. Gordon, and J. E. Johnson, 2002: Measurements of aerosol vertical profiles and optical properties during INDOEX 1999 using micro-pulse lidars. *J. Geophys. Res.*, in press.

Welton, E. J., J. R. Campbell, J. D. Spinhirne, and V. S. Scott, 2001: Global monitoring of clouds and aerosols using a network of micro-pulse lidar systems. In *Lidar Remote Sensing for Industry and Environmental Monitoring*, U. N. Singh, T. Itabe, N. Sugimoto, (eds.), *Proc. SPIE*, **4153**, 151-158.

Welton, E.J., and J.R. Campbell, 2002: Micro-pulse lidar signals: Uncertainty analysis. *J. Atmos. Oceanic Technol.*. Submitted.

Welton, E. J., J. R. Campbell, S. P. Palm, D. L. Hlavka, W. D. Hart, and J. D. Spinhirne, 2002: Calibration techniques and uncertainty studies for ground-based and space-based elastic backscatter lidar systems. *Appl. Opt.*, Submitted.

Table Captions

Table 1. Dates of operation, uptime percentages (based on 24 hr/day operation) and temporal/spatial resolution settings for the MPL instrument during ARREX and SAFARI-2000.

Figure Captions

Figure 1. Outdoor MPL environment-controlled operating containers used for ARREX (a), and indoor logistical arrangement during SAFARI-2000 (b).

Figure 2. Automated surface aerosol processing algorithm output for the period 18 August – 13 September 2000 (fractional days 231 – 257 inclusive). Calculated layer-mean S-ratio values for surface-detached aerosol layer with uncertainty bars (top), corresponding CIMEL 523-interpolated aerosol optical depths (top-middle) and Angstrom exponents (bottom-middle), and the derived aerosol layer top height used to initiate algorithm inversion techniques (bottom).

Figure 3. For the period 15 August through 15 September, the average aerosol optical depth versus average Angstrom exponent from available CIMEL sun-photometer data during 1998 – 2001 at Skukuza.

Figure 4. Corresponding to Fig. 2, a comparison of Angstrom exponent values calculated from available CIMEL sun-photometer measurements vs. algorithm derived layer-mean S-ratio values (a), and CIMEL 523 nm interpolated aerosol optical depths (b).

Figure 5. A comparison of the measured diffuse to direct broadband flux ratio versus corresponding path-normalized CIMEL 523 nm interpolated aerosol optical depth

for three groups of calculated S-ratio values; less than 55 (+), between 55 and 75 (*) and greater than 75 (o).

Figure 6. MODIS Level 1B geo-located RGB composite imagery from bands 1, 4 and 3 (.66 μm, .55 μm, and .47 μm) for northeastern South Africa from 0900 – 0905 UTC, September 1, 2000. The Skukuza Airport site (24.97° S, 31.58° E) is denoted by the white dot.

Figure 7. MPL Normalized Relative Backscatter (counts*km^2/uj*usec) from 1 September 2000 at the Skukuza Airport site.

Figure 8. Balloonsonde profiles of temperature versus height above ground (km) from 1 September 2000 at approximately 0500 UTC (fractional day 245.2076) (a), and 1200 UTC (245.4993) (b) launched at the Skukuza Airport site.

Figure 9. For daylight hours (approximately 0500 – 1500 UTC) on 1 September 2000, top displays total (blue dots), direct (red dots) and diffuse (green dots) broadband flux measurements, scaled 866 nm multi-filter shadowband radiometer AOD values (violet +'s), and scaled airmass values (blue +'s) (a). Bottom shows total measured broadband flux versus airmass (b). Circles represent measurements as sun was rising. Crosses indicate measurements as the sun was setting. Radiative forcing of afternoon smoke layer can be interpreted by comparing corresponding airmass measurements (i.e. early morning and late afternoon). The forcing in this case is estimated to be greater than – 50 W/m^2.

Figure 10. Corresponding to Fig. 2 but expanded for 1 September 2000.

Figure 11. MPL-derived extinction cross-section profiles with uncertainty bars versus height above ground (km) for 30-min data periods on 1 September 2000; 0530 UTC (fractional day 245.2281) (a), 1200 UTC (245.5011) (b) and 1435 UTC (245.6071).

Figure 12. MPL Normalized Relative Backscatter (counts*km^2/uj*usec) from 7 September 1999 at the Skukuza Airport site. Aerosol structure can be clearly seen up to 12 km above ground level.

Experiment	Unit #	Dates	Uptime	ΔV	ΔT
ARREX	68	14 August – 10 September 1999	90%	30 m	60s
SAFARI-2000	66	17 August – 20 September 2000	92%	75 m	60s

Table 1

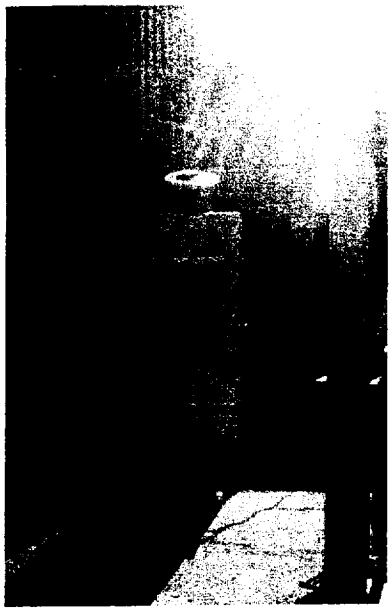

Figure 1a

PURPOSELY BLANK – AWAITING FINAL PICTURE

Figure 1b

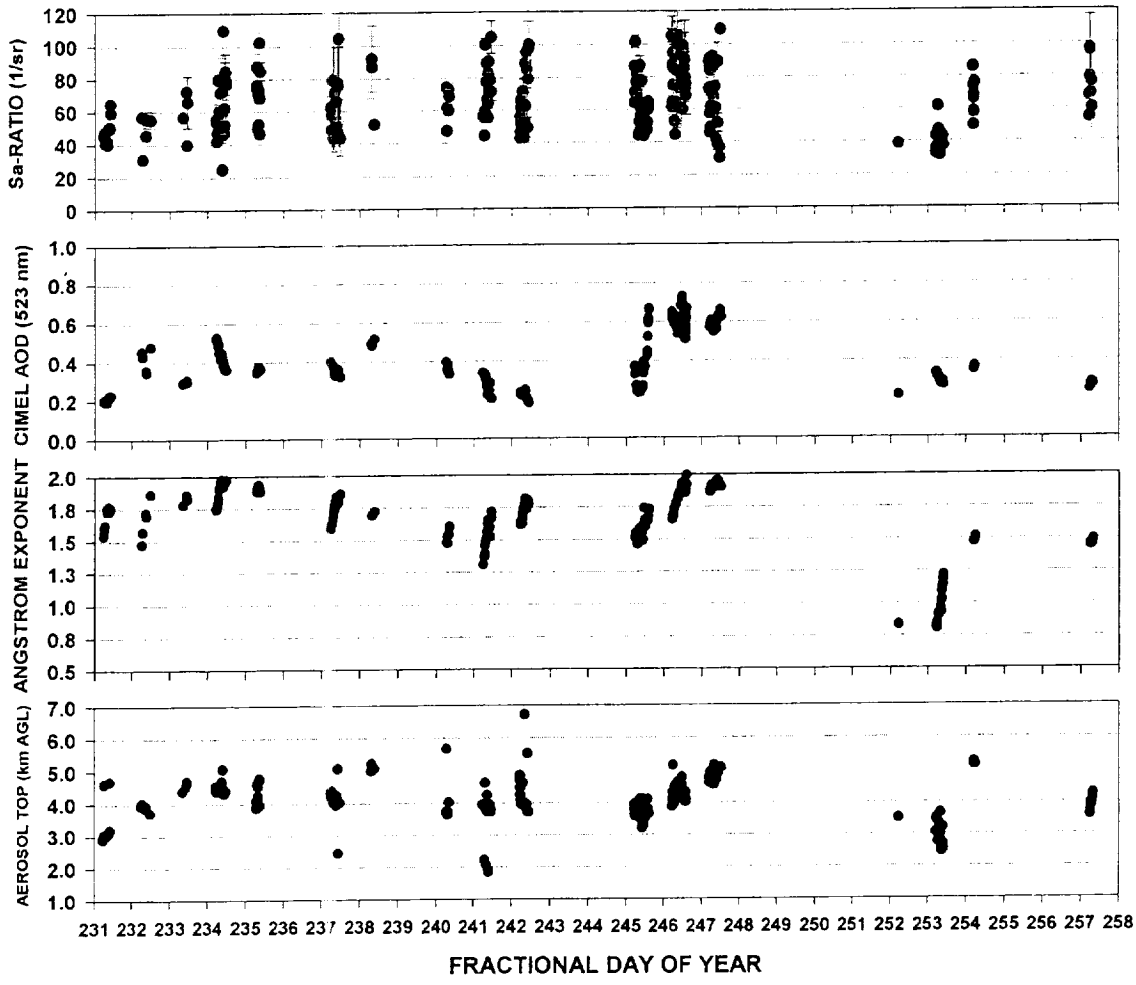
Sa-RATIO (1/sr)
120
100
80
60
40
20
0
CIMEL AOD (523 nm)
1.0
0.8
0.6
0.4
0.2
0.0
ANGSTROM EXPONENT
2.0
1.8
1.5
1.3
1.0
0.8
0.5
AEROSOL TOP (km AGL)
7.0
6.0
5.0
4.0
3.0
2.0
1.0
231 232 233 234 235 236 237 238 239 240 241 242 243 244 245 246 247 248 249 250 251 252 253 254 255 256 257 258
FRACTIONAL DAY OF YEAR

Figure 2

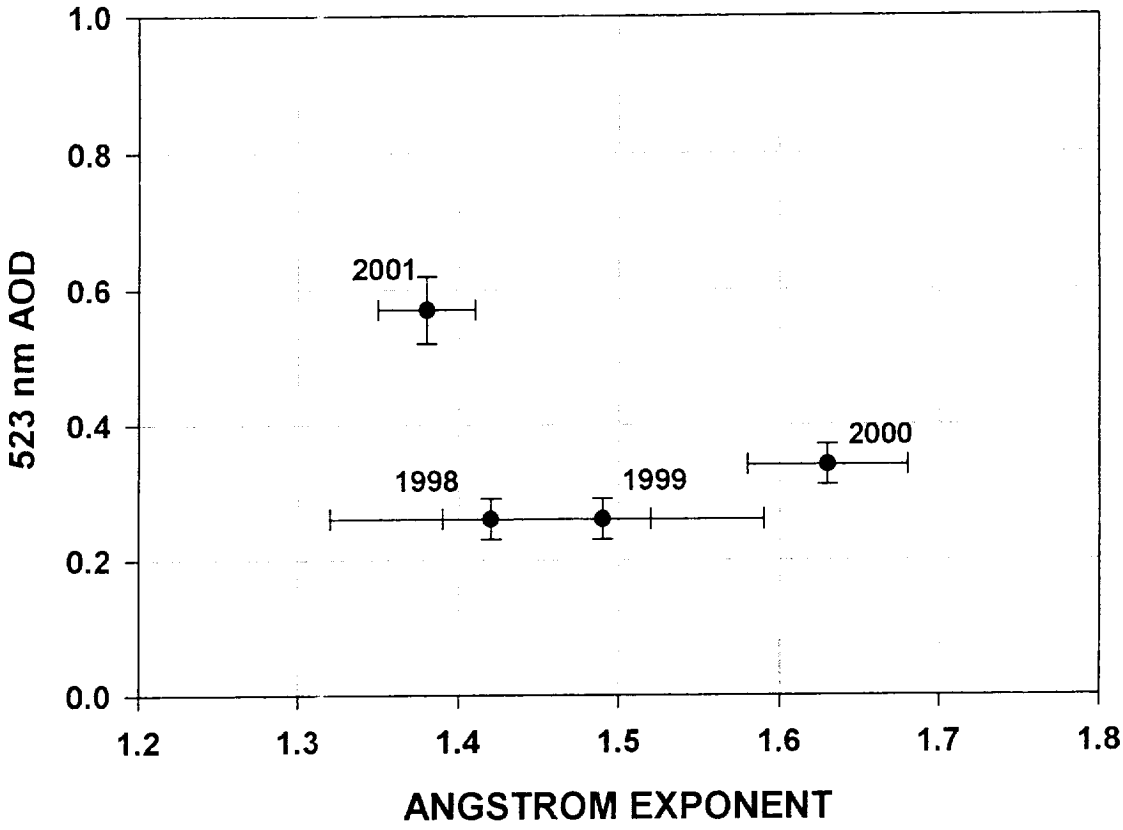
1.0
0.8
0.6
0.4
0.2
0.0
523 nm AOD
2001
2000
1998
1999
1.2
1.3
1.4
1.5
1.6
1.7
1.8
ANGSTROM EXPONENT

Figure 3

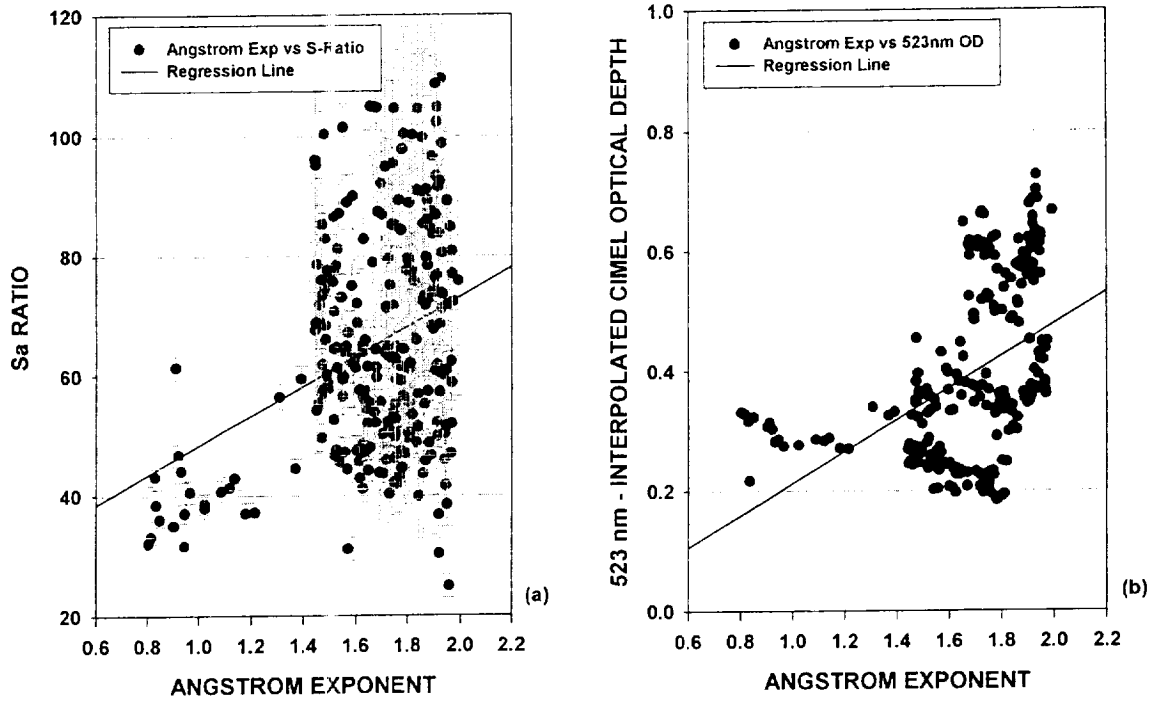
Angstrom Exp vs S-Ratio
Regression Line
Sa RATIO
ANGSTROM EXPONENT
(a)
Angstrom Exp vs 523nm OD
Regression Line
523 nm - INTERPOLATED CIMEL OPTICAL DEPTH
ANGSTROM EXPONENT
(b)

Figure 4

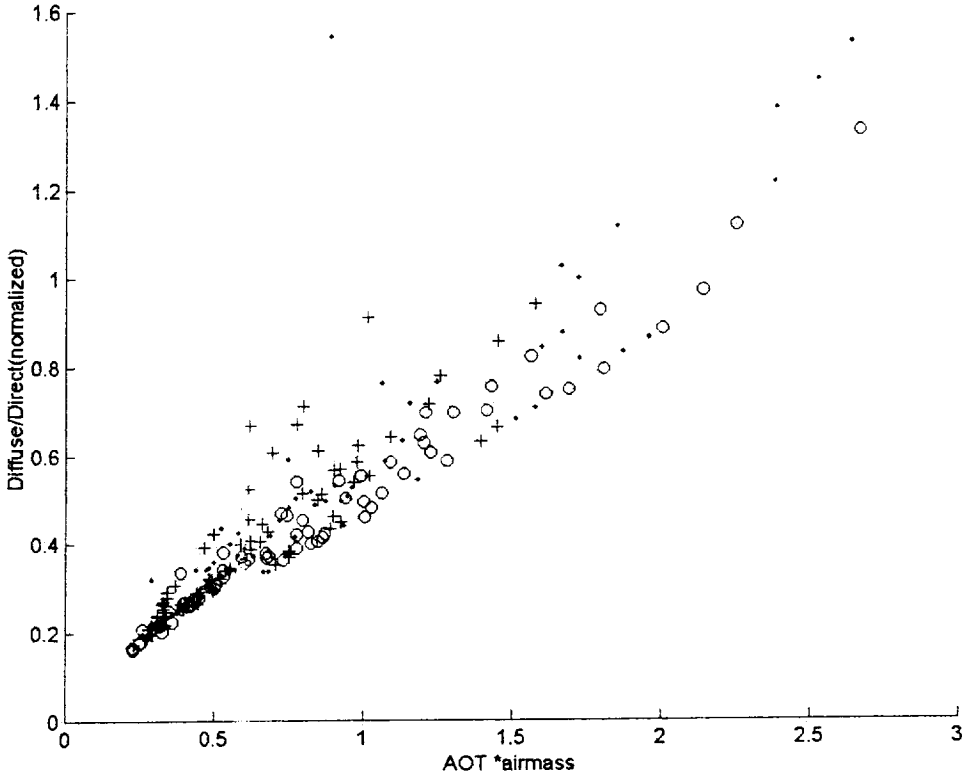
Diffuse/Direct(normalized)
AOT *airmass
0
0.2
0.4
0.6
0.8
1
1.2
1.4
1.6
0.5
1.5
2
2.5
3

Figure 5

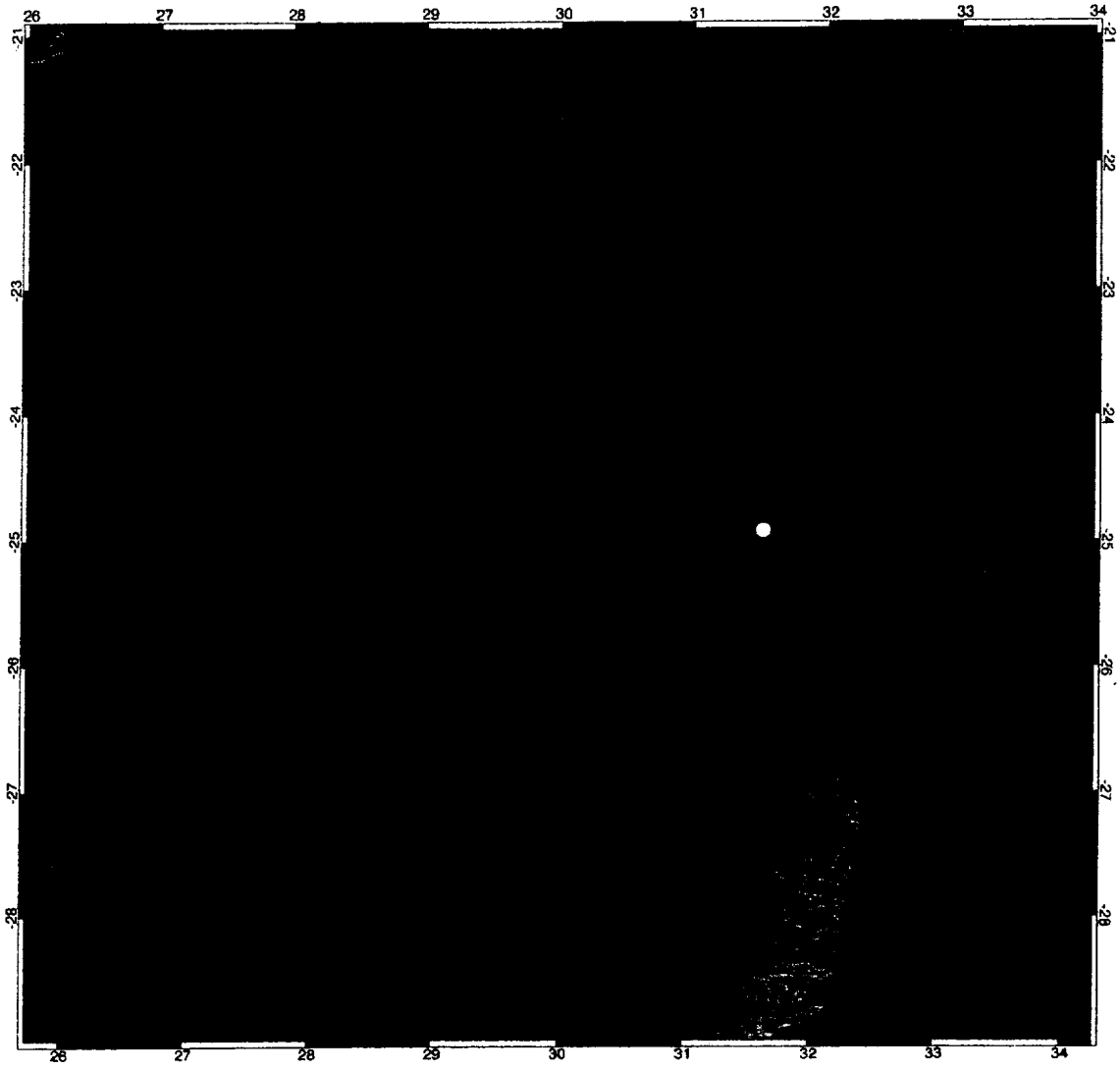

Figure 6

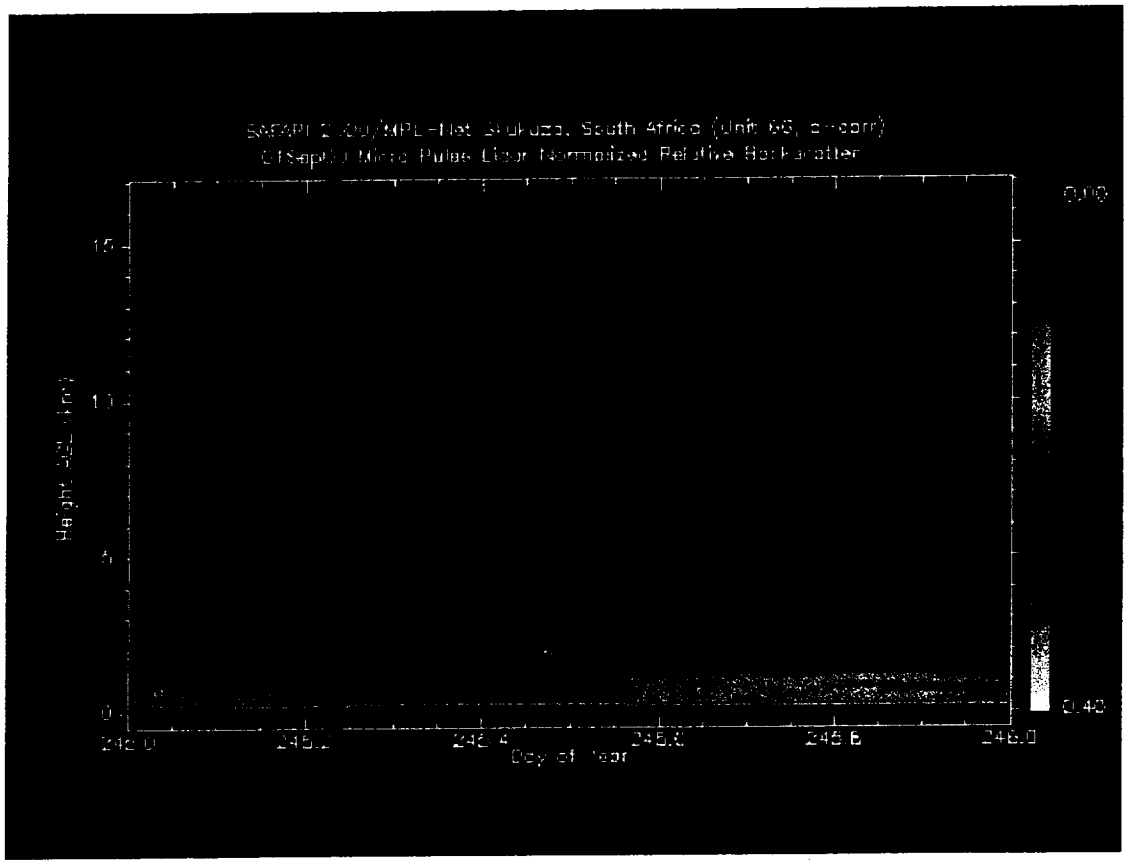

Figure 7

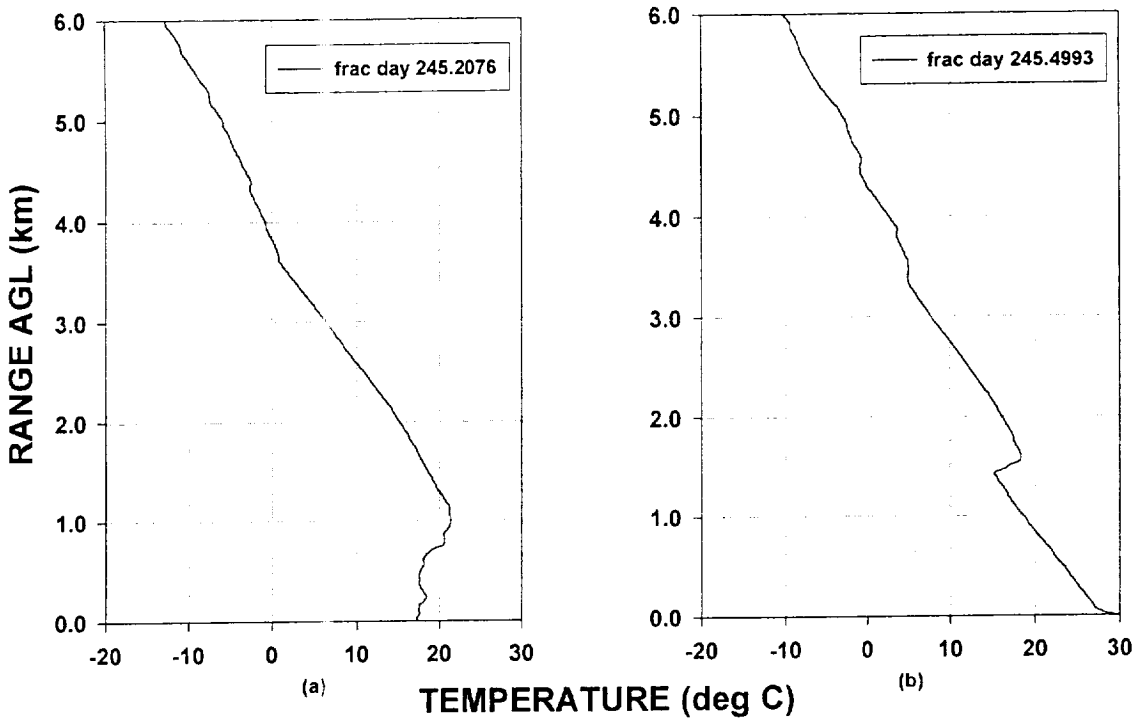
RANGE AGL (km)
6.0
5.0
4.0
3.0
2.0
1.0
0.0
frac day 245.2076
-20
-10
0
10
20
30
(a)
frac day 245.4993
(b)
TEMPERATURE (deg C)

Figure 8

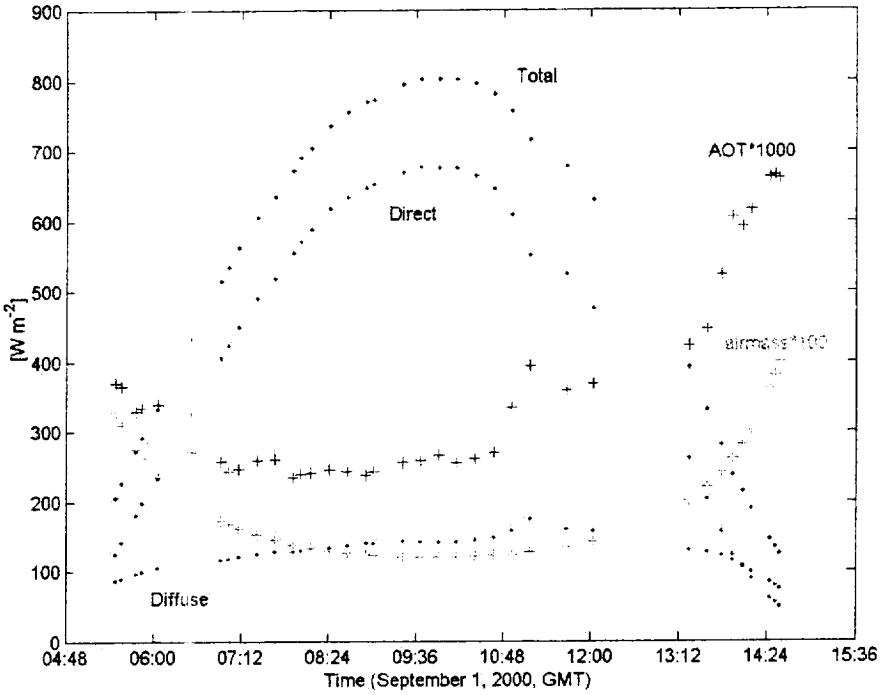
Total
AOT*1000
Direct
airmass*100
Diffuse
[W m-2]
Time (September 1, 2000, GMT)
04:48
06:00
07:12
08:24
09:36
10:48
12:00
13:12
14:24
15:36

(a)

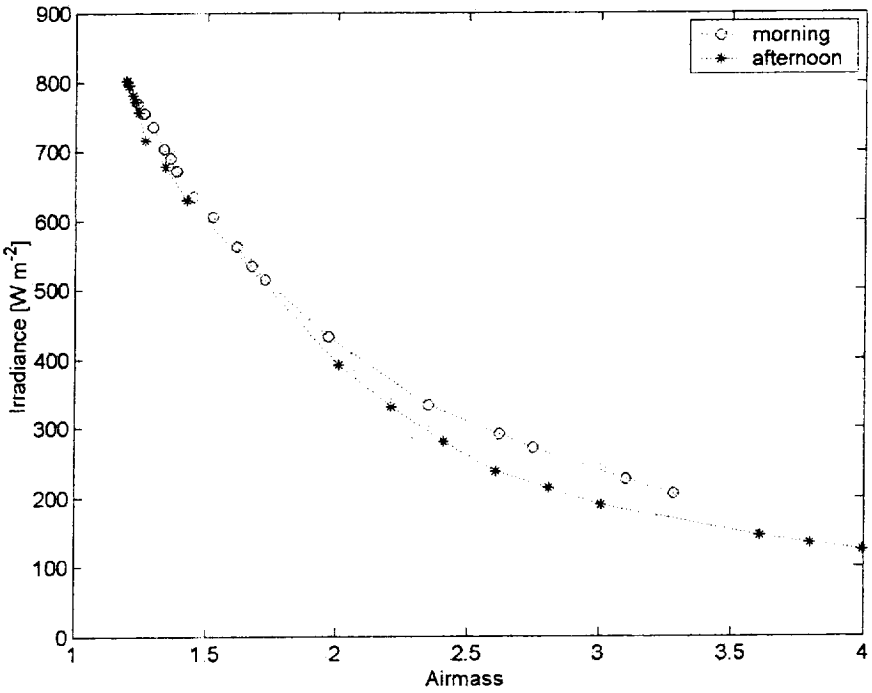
morning
afternoon
Irradiance [W m-2]
Airmass

(b)

Figure 9

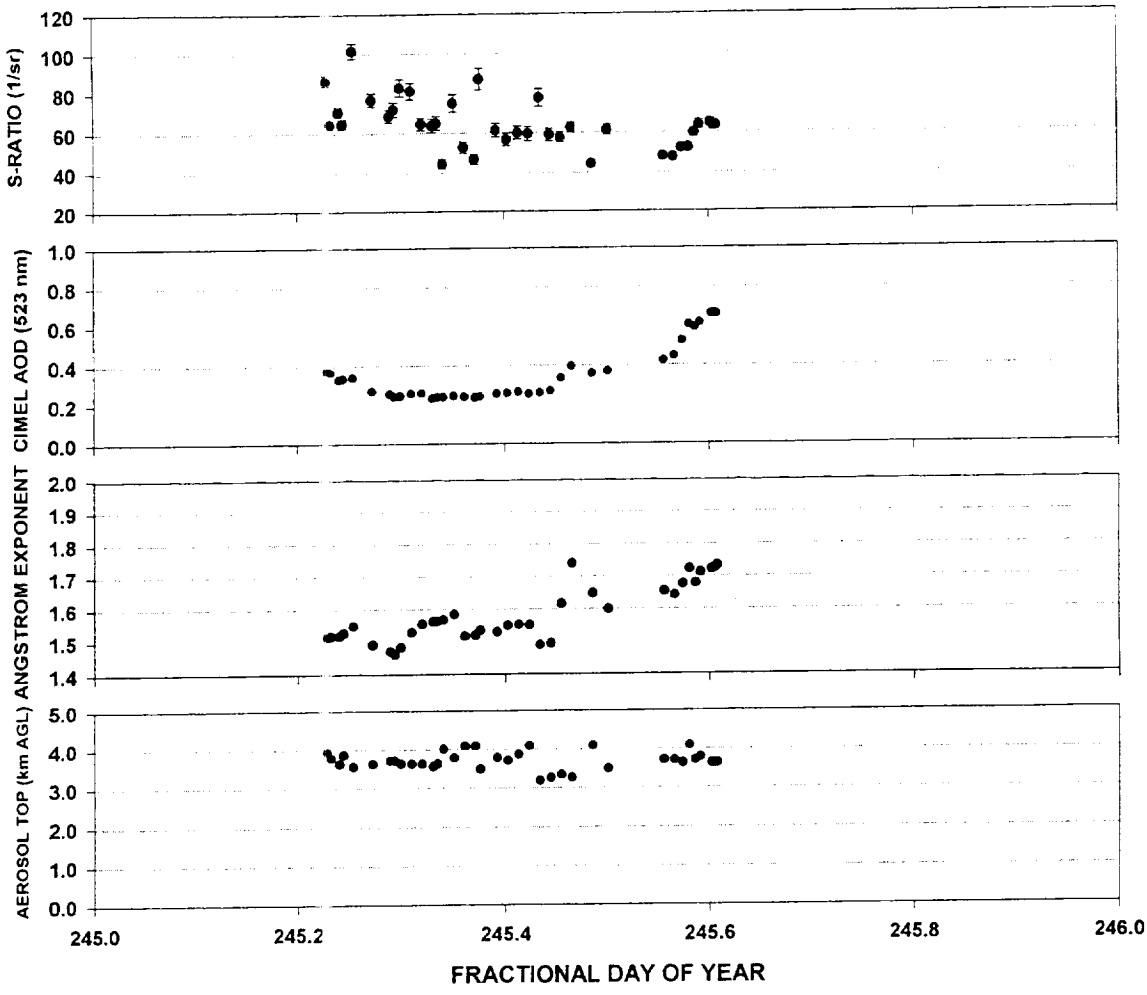
S-RATIO (1/sr)
120
100
80
60
40
20
CIMEL AOD (523 nm)
1.0
0.8
0.6
0.4
0.2
0.0
ANGSTROM EXPONENT
2.0
1.9
1.8
1.7
1.6
1.5
1.4
AEROSOL TOP (km AGL)
5.0
4.0
3.0
2.0
1.0
0.0
245.0
245.2
245.4
245.6
245.8
246.0
FRACTIONAL DAY OF YEAR

Figure 10

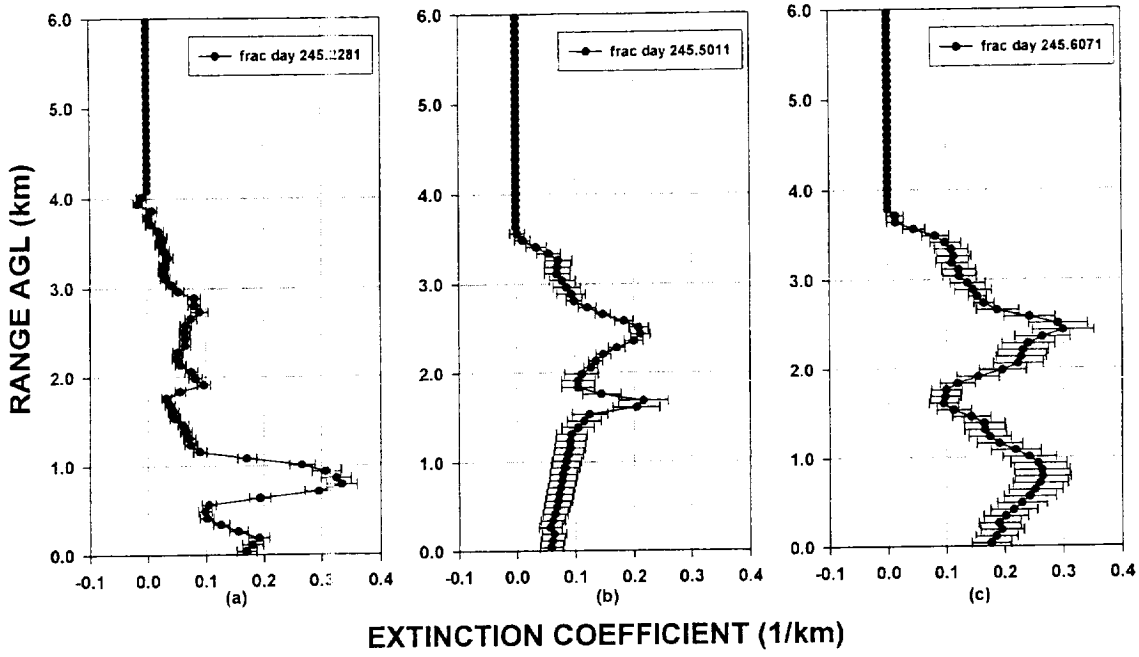
RANGE AGL (km)
frac day 245.6281
frac day 245.5011
frac day 245.6071
(a)
(b)
(c)
EXTINCTION COEFFICIENT (1/km)

Figure 11

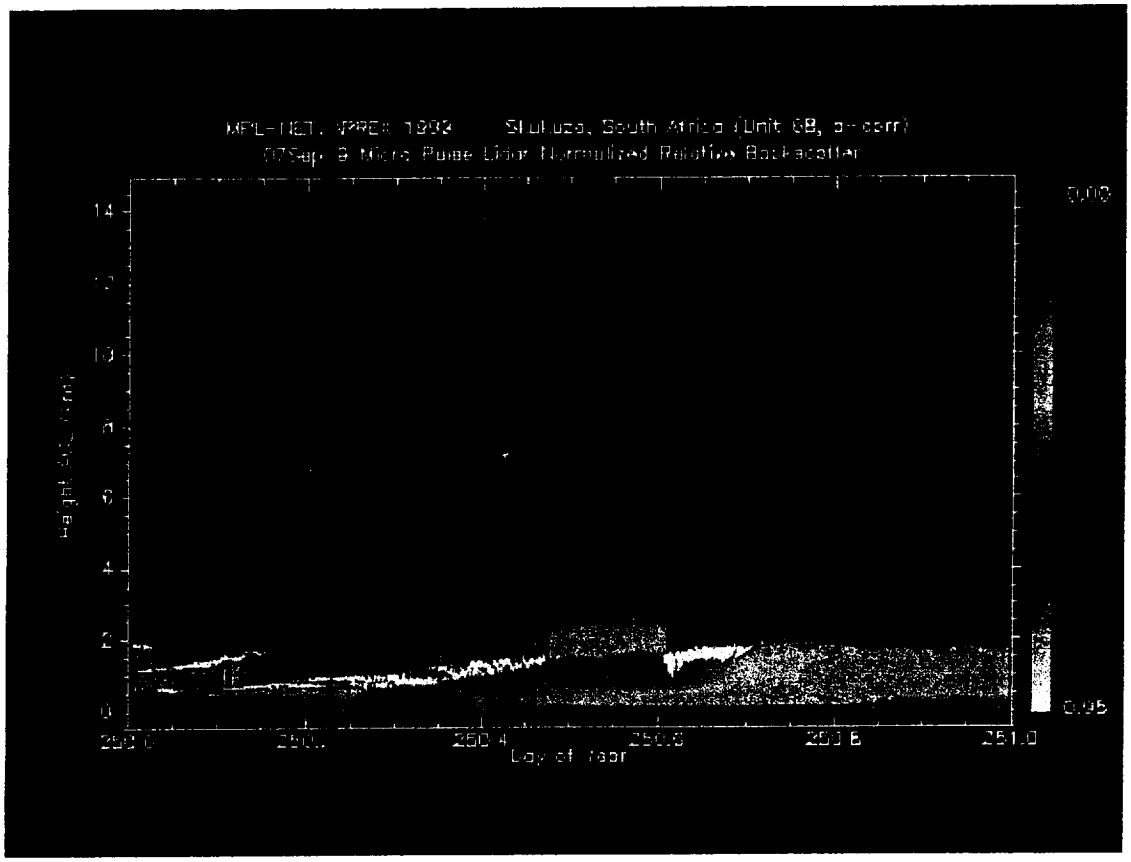
MPL-NET, VPRC: 1999 Sluluza, South Africa (Unit 68, a-corr)
07Sep: 8 Micro Pulse Lidar Normalized Relative Backscatter
0.09
0.05
14
12
10
8
6
4
2
0
250.2
250.4
250.6
250.8
251.0
Day of Year

Figure 12